Biochimica et Biophysica Acta 1833 (2013) 1421–1433

Contents lists available at SciVerse ScienceDirect

Biochimica et Biophysica Acta

journal homepage: www.elsevier.com/locate/bbamcr

Direct association of the reticulon protein RTN1A with the ryanodine receptor 2 in neurons

Levent Kaya [a], Barbara Meissner [a], Maria Christine Riedl [b], Martin Muik [b], Christoph Schwarzer [c], Francesco Ferraguti [c], Bettina Sarg [d], Herbert Lindner [d], Rüdiger Schweigreiter [a], Hans-Günther Knaus [e], Christoph Romanin [b], Christine E. Bandtlow [a,*]

[a] Division of Neurobiochemistry, Biocenter, Innsbruck Medical University, Innsbruck, Austria
[b] Institute of Biophysics, University of Linz, 4040 Linz, Austria
[c] Institute of Pharmacology, Innsbruck Medical University, Innsbruck, Austria
[d] Division of Clinical Biochemistry, Innsbruck Medical University, Innsbruck, Austria
[e] Department for Medical Genetics, Molecular and Clinical Pharmacology, Innsbruck Medical University, Innsbruck, Austria

ARTICLE INFO

Article history:
Received 15 November 2012
Received in revised form 11 February 2013
Accepted 14 February 2013
Available online 27 February 2013

Keywords:
Reticulon
Brain
Protein–protein interaction
Calcium homeostasis

ABSTRACT

RTN1A is a reticulon protein with predominant localization in the endoplasmic reticulum (ER). It was previously shown that RTN1A is expressed in neurons of the mammalian central nervous system but functional information remains sparse. To elucidate the neuronal function of RTN1A, we chose to focus our investigation on identifying possible novel binding partners specifically interacting with the unique N-terminus of RTN1A. Using a nonbiased approach involving GST pull-downs and MS analysis, we identified the intracellular calcium release channel ryanodine receptor 2 (RyR2) as a direct binding partner of RTN1A. The RyR2 binding site was localized to a highly conserved 150-amino acid residue region. RTN1A displays high preference for RyR2 binding *in vitro* and *in vivo* and both proteins colocalize in hippocampal neurons and Purkinje cells. Moreover, we demonstrate the precise subcellular localization of RTN1A in Purkinje cells and show that RTN1A inhibits RyR channels in [^{3}H]ryanodine binding studies on brain synaptosomes. In a functional assay, RTN1A significantly reduced RyR2-mediated Ca^{2+} oscillations. Thus, RTN1A and RyR2 might act as functional partners in the regulation of cytosolic Ca^{2+} dynamics the in neurons.

1. Introduction

Reticulons (RTNs) are a highly conserved eukaryotic protein family residing in the endomembrane system. In mammals 4 reticulon genes are known (RTN1–RTN4), which encode various protein isoforms [1,2]. Reticulons share little sequence homology except for the reticulon homology domain (RHD), a C-terminally located domain of ~200 amino acids composed of two short hairpin domains separated by a highly conserved loop-region. While their physiological relevance is still poorly understood, recent findings suggest that reticulons partition into tubules of the ER *via* their RHD and act as membrane curvature proteins responsible for shaping ER-tubules and ER-sheet edges. Moreover, by interacting with other hairpin loop-containing proteins, such as REEP1, atlastin-1 and M1 spastin, RTNs appear to participate in a network of ER morphogens [3].

In the mammalian nervous system the role of RTNs remains unclear, though a variety of functions have been postulated for specific RTNs, including vesicular and membrane trafficking [4], neuroendocrine secretion [5], hereditary spastic paraplegia [6], inhibition of enzymatic activity [7], apoptosis [8,9], and regulation of axonal growth and plasticity [10]. RTN1A, the longest isoform of the rtn1 gene, was the first RTN protein described to be widely expressed in the developing and mature brain [11,12]. As opposed to the well studied Nogo/RTN4 proteins, RTN1A in the adult brain is located exclusively in the neurons but not in the glial cells [11]. RTN1C was shown to interact with Spastin [13], Sec61 [14] and AP-2 [15] suggesting that it might be involved in regulating intracellular vesicle transport, although a firm conclusive answer is missing. While these interactions are mediated *via* the C-terminal RHD, common to all RTNs, little is known about the variable N-terminal regions, specific for each RTN isoform. Assuming that the N-terminal domains are specialized for distinct functions by associating with different target proteins, we have set out to search for binding proteins that specifically bind to the N-terminal domain of neuronal RTN1A. Using a GST pull-down and co-immunoprecipitation strategy, we demonstrate for the first time that in rodent brain RTN1A forms a stable association with the ryanodine receptor RyR2, but not the closely related family member RyR1 and that this interaction was found to modify RyR2 channel function, as judged

Abbreviations: RTN, reticulon protein; ER, endoplasmic reticulum; RyR, ryanodine receptor; RHD, reticulon homology domain; CICR, calcium induced calcium release; IPTG, isopropyl-β-d-thiogalactopyranoside; PB, phosphate buffer; DAB, 3,3′-diaminobenzidine tetrahydrochloride dihydrate; CA, cornu ammonis

* Corresponding author at: Innsbruck Medical University, Biocenter, Division of Neurobiochemistry, Innrain 80/82, A-6020 Innsbruck, Austria. Tel.: +43 512 900370280.
E-mail address: christine.bandtlow@i-med.ac.at (C.E. Bandtlow).

0167-4889
http://dx.doi.org/10.1016/j.bbamcr.2013.02.012

from ryanodine binding experiments and single cell calcium imaging analysis. Our observations suggest that RyR2 channels may form stable interactions with RTN1A, leading to a reduction of RyR2-mediated Ca^{2+} oscillations.

RyR2 is a member of the intracellular ryanodine receptor Ca^{2+}-release channels (RyRs) localized in the ER. Three RyR isoforms have been purified in mammals (RyR1, RyR2 and RyR3) that coordinate many calcium signaling events such as muscle contraction and neurotransmission. RyR1 is predominant in the skeletal muscle and in the cerebellar Purkinje neurons. RyR2 is mainly expressed in the cardiac muscles and is the predominant subtype in the brain, while the brain specific RyR3 is weakly expressed throughout the brain [16]. RyRs contribute to the regulation of the cytosolic calcium dynamics, by release of calcium from intracellular Ca^{2+} stores as a consequence of Ca^{2+} influx through voltage- or ligand-gated Ca^{2+} channels, the so-called Ca^{2+}-induced Ca^{2+} release (CICR) [17]. CICR from the intracellular calcium stores that amplifies further the Ca^{2+} signal is thought to be involved in more profound and lasting changes in neurons, regulating neurotransmitter release, synaptic plasticity, gene expression, and signal transduction to the nucleus [18]. Recent evidence supports a role of RyR2-mediated control of calcium homeostasis in stress-induced defects in cognitive function and postsynaptic plasticity in hippocampal neurons [19]. Moreover, leaky neuronal RyR2 channels are also implicated in neurodegeneration, including Alzheimer's disease and aging.

2. Materials and methods

2.1. Plasmid constructs

pcDNA3.1-RyR2 containing full length mouse cardiac RyR2 cDNA, GenBankTM accession no. NP_076357.2 was kindly provided by Wayne Chen (University of Calgary, Calgary; [20]), and a pCI-neo vector (Promega) with a full length rabbit skeletal RyR1 insert (GenBank accession no. X15209) was kindly provided by P. D. Allen (Brigham and Women's Hospital, Boston; [21]). GST-RTN1$_{523}$ (aa 1–523; 5′-CTGGGATCCATGGCCGCA CCGCCGGATCTGCAAG-3′ forward and 5′-CAGCCCGGGTCAATGATGATGATGATGAT GACCACGCTGAGTATCGGGTCAGGTTCCACAG-3′ reverse and GST-HHD (aa 376–523; 5′-AATGGATCCCCAGTG GGCCAGGCGGCCGAC-3′ forward) and 5′-CAGCCCGGGTC AATGATGAT GATGATGATGACCACCGCTGAGTATCGGGTCAGGTTCCACAG-3′ reverse) were generated by PCR amplification using rat full length RTN1A as a template [2], and cloned into pGEX-6P (Amersham Pharmacia). GST-LNT1 (aa 1–375, 5′-CTGGGATCCATGG CCGCACCGCCGGATCTGCA AG-3′ forward and 5′-TCAATGATGATGATGATGATGCACTGGCCTTGGA CTCTCGGTTG-3′ reverse) was generated by PCR amplification using GST-RTN1$_{523}$ as a template and cloned into pGEX-6P. GST-NiR was described previously [22]. mCherry-RTN1$_{523}$ (5′-ACGAAGCTTCGCC ACCATGGTGATGGCCGCACCGCCGGATCTG CAAG-3′ forward and 5′-TGCGGATCCGCGCTGAGTATCGGGTCAGGTTCCACAG-3′ reverse) was generated *via* PCR amplification using rat RTN1A-eGFP as template and cloned into mCherryN (Clontech). Restriction sites used for subcloning are underlined. All constructs were verified by sequencing analysis (MWG, Ebersberg, Germany).

2.2. Expression and purification of recombinant GST fusion proteins

Recombinant protein expression of transformed *E. coli* (BL21(DE3)) cells was induced with 1 mM IPTG (isopropyl-β-d-thiogalactopyranoside) for 4 h at 20 °C. Cells were then harvested by centrifugation and 1 g of bacterial pellet was resuspended in 4 mL of lysis buffer (50 mM sodium phosphate buffer, pH 7.4, 150 mM NaCl, 0.1% Triton X-100, 0.05% Tween-20) supplemented with Lysozyme (1 mg/mL), Protease Inhibitor Cocktail (Roche) and DNAse (0.1 mg/mL). The lysate was sonicated 5 times for 15 s each (on ice) and was then cleared by centrifugation at 15,000 ×*g* for 15 min at 4 °C. For dual purification, the precleared supernatant was first run over a GSTrap Affinity Column (GE Healthcare) attached to a chromatography apparatus (ÄKTA prime, GE Healthcare). Bound proteins were eluted with 50 mM reduced glutathione in TBS, pH 8.0 containing 0.1 mM β-mercaptoethanol. GST-purified eluate was collected, and subjected on a HisTrap Affinity Column (GE Healthcare). Bound protein was eluted with wash buffer (50 mM sodium phosphate buffer at pH 7.4, 0.1% Triton X-100, 0.05% Tween-20, 150 mM NaCl) containing imidazole at a final concentration of 500 mM. Samples of the eluated tagged purified recombinant proteins were analyzed by SDS-PAGE and Silver Staining [23,24] and immobilized to Glutathione Sepharose Beads (GE Healthcare) for 2 h at 4 °C.

2.3. GST pull-down assays

For *in vitro* GST pull-down assays, whole adult mouse brains (BL6, 10 weeks) were homogenized by 50 strokes of a dounce homogenizer in ice-cold lysis buffer (50 mM HEPES pH 7.4, 25 mM NaCl, 10 mM EDTA, 1% Triton X-100) and complete protease and phosphatase inhibitor cocktail (Roche; 1:10; w/v). The homogenate was centrifuged for 30 min at 20,000 ×*g*, 4 °C and supernatant was passed through a 0.45 μm filter (BD Biosciences). 40 mg of total brain extract (10 mg/mL) was precleared by incubation for 2 h at 4 °C with 0.20 mL of glutathione agarose followed by centrifugation (500 ×*g* for 2 min) and assayed for protein content. 2.5 mg of the recovered brain extract (2.5 mg/mL) was incubated overnight at 4 °C with indicated concentrations of recombinant GST-fusion proteins immobilized to Glutathione Sepharose Beads (GE Healthcare). GST or Glutathione agarose (0.2 mL) served as controls. Agarose beads were washed five times in lysis buffer at 4 °C and resuspended in Laemmli sample buffer. Samples were separated by 12.5% SDS-PAGE, and analyzed by silver staining or immunoblotting using standard procedures.

2.4. MS analysis

For MS analysis, silver stained protein bands were cut out and subjected to in-gel digestion as published previously [25]. Protein digests were analyzed using an UltiMate 3000 nano-HPLC system (Dionex, Germering, Germany) coupled to an LTQ Orbitrap XL mass spectrometer (ThermoScientific, Bremen, Germany) equipped with a nanospray ionization source. A homemade fritless fused silica microcapillary column (75 μm i.d. × 280 μm o.d.) packed with 10 cm of 3 μm reverse-phase C_{18} material (Reprosil) was used. The gradient (solvent A: 0.1% formic acid; solvent B: 0.1% formic acid in 85% acetonitrile) started at 4% B. The concentration of solvent B was increased linearly from 4% to 50% during 50 min and from 50% to 100% during 5 min. A flowrate of 250 nL/min was applied. Protein identification was performed using the Mascot search engine and the NCBInr database (mus) accepting variable modifications, carbamidomethyl (C), oxidation (M). Specific cleavage sites for trypsin (KR) were selected with two missed cleavage sites allowed. Peptide tolerance was ±10 ppm and MS/MS tolerance was ±1 Da. Peptides with a Mascot score below 30 were skipped. Only best matches were considered.

2.5. Co-immunoprecipitation and immunoblotting

Total brain extract was prepared from adult Sprague–Dawley cerebella in a manner similar to the GST pull-down experiments. 1 mg of cleared lysate (4 mg/mL) was then incubated for 1 h at 4 °C with 5 μg of either mouse anti-RyR2 (Clone c3-33, Pierce), mouse anti-RTN1A (MON162; MuBio, Netherlands), mouse anti-RTN4A (clone 11C7; 22), rabbit anti-RTN1A [2], rabbit anti-RTN4 [22] or rabbit IgG (Sigma). 25 μL of Protein G Dynabeads (Invitrogen) were then added for 1 h and rotated at 4 °C. Beads were washed five times in lysis buffer at 4 °C and were removed from the supernatant using Dynal Magnetic Particle concentrators (Invitrogen). Beads were boiled in Laemmli sample buffer and samples were loaded on 6% SDS-PAGE gels and blotted onto PVDF membranes (GE Healthcare). After staining with Ponceau S

(Sigma-Aldrich) to visualize proteins, membranes were blocked in 5% Skim-Milk (Merck) in TBS-Tween 20 (TBS-T; 10 mM Tris-base, 150 mM NaCl, and 0.2% Tween 20, pH8.0) for 2 h at RT. Wherever feasible, the PVDF membranes were probed with antibodies different from those used for immunoprecipitation to maximize the specificity of the immunoreactive product obtained. For RTN1A in particular, we used either of two antibodies highly specific for RTN1A: a rabbit antibody specific for the cytoplasmic domain of RTN1A (1:100,000; [2]) and a monoclonal one raised against amino acids 338–422 of RTN1A (MON162; 1:1000; MuBio, Netherlands). RyR2 was identified with a mouse antibody recognizing all RyR isoforms (1:1000; Pierce), RyR1 with rabbit anti-RyR1 (1:1000; Alomone Labs, Israel), IP3R1 with rabbit anti-IP3R1 (1:4000; Alomone Labs, Israel) and RTN4A with either rabbit or mouse anti-RTN4A [22]. Primary antibody incubation was performed at RT for 2 h followed by several washing steps in TBST-T. Antibody binding to proteins was detected using secondary antibody conjugated to horseradish peroxidase (1:20,000; Thermo Scientific) and visualized by enzyme-linked chemiluminescence using ECL Detection Kit (Amersham), and a Typhoon Scanner Device (Amersham Biosciences).

2.6. HEK293 cell culture and transfection

HEK293 cells were maintained in Dulbecco's modified Eagle's Medium-High Glucose as previously described and transfected with 2–10 μg mouse RyR2 or rabbit RyR1 cDNAs with or without 0.2–1 μg rat RTN1A-myc, RTN4A-myc, $RTN1_{523}$-mCherry or mCherry cDNAs using Ca^{2+} phosphate precipitation [26]. Cells were either lysed 40 h post-transfection and processed for immunoprecipitation as described above or fixed in 4% paraformaldehyde for 15 min, permeabilized in 0.1% Triton-X100 in PBS for 20 min and immunostained using mouse monoclonal antibodies against RyR2 (1:1000; Clone c3-33, Pierce), or RyR1 (1:500; Alomone Labs, Israel), followed by subsequent detection using secondary antibodies conjugated to Alexa488 (1:1000; Invitrogen). Single cells transfected with untagged RyR1 or RyR2 were double stained with rabbit anti-calreticulin (1:500; Abcam) and mouse pan-RyR antibody (1:1000; Pierce). Images were captured using a Leica SP5 microscope and a Leica PL APO 63×/1.4 oil-immersion lens. Quantification of colocalization depicted is an average of 10 independent cells per group. Colocalization and quantification were performed using Pearson's coefficient of colocalization of red and green fluorescent signals captured of the same microscopy field, using the LAS AF software (Leica, Mannheim, Germany).

2.7. Ca^{2+}-imaging

Transfection of HEK cells [27] was performed using TransFectin (Biorad, Germany) with the corresponding plasmids, *i.e.* 2 μg RyR2, 0.2 μg mcherry or 0.3 μg of either mcherry-RTN1A or EGFP-RTN4A. Measurements were carried out 24 to 48 h following transfection. Employing Fura-2 microscopy, transfected HEK293 cells grown on coverslips for 1–2 days were loaded with Fura-2/AM (1 μM) for 30 min at room temperature in an extracellular, nominally Ca^{2+} free solution (0 mM Ca^{2+}: 140 NaCl, 5 KCl, 1 $MgCl_2$, 10 glucose, 10 Hepes, pH 7.4 (NaOH)) and mounted at an inverted Axiovert 100 TV microscope (Zeiss, Germany). Excitation of Fura-2 was performed at 340 nm and 380 nm, and Ca^{2+} measurements are shown as 340/380 ratios of transfected HEK293 cells which were corrected for EGFP crossexcitation in the case of EGFP-RTN4A. To evoke Ca^{2+} oscillations according to [28] the nominally Ca^{2+} free solution was exchanged by a 1 mM Ca^{2+} extracellular solution (140 NaCl, 5 KCl, 1 $MgCl_2$, 1 $CaCl_2$, 10 glucose, 10 Hepes, pH 7.4 (NaOH)). The amount of Ca^{2+} released during oscillations over a 450 s time-period was estimated by the cumulative area of the oscillations peaks. Transfected HEK293 cells were identified by their mcherry or EGFP fluorescence and a response to 10 mM caffeine in nominally Ca^{2+}-free solution which was taken as an indicator for RyR2 expression.

2.8. Animals, tissue preparation and immunohistochemistry for light and electron microscopy

Adult male Sprague Dawley rats (300–400 g; Dept. Laboratory Animals and Genetics, Medical University Vienna, Vienna, Austria) were used for light and electron microscopy experiments. All experimental protocols were approved by the Austrian Animal Experimentation Ethics Board in compliance with both the European Convention for the Protection of Vertebrate Animals used for Experimental and Other Scientific Purposes (ETS no. 123) and the European Communities Council Directive of 24 November 1986 (86/609/EEC). Every effort was made to minimize the number and suffering of the animals used. Animals were deeply anesthetized by intraperitoneal injection of thiopental (100 mg/kg, i.p.) and perfused transcardially with phosphate buffered saline (PBS; 25 mM, 0.9% NaCl, pH 7.4) followed for 15 min by ice-cold fixative made of 4% w/v paraformaldehyde, for light microscopy experiments, or with the addition of 15% v/v of a saturated solution of picric acid and 0.05% glutaraldehyde immediately before the perfusion for pre-embedding electron microscopy. Brains were then immediately removed from the skull, washed in 0.1 M phosphate buffer (PB) and sliced coronally in 40 or 70 μm thick sections on a vibratome (Leica Microsystems VT1000S, Vienna, Austria). Sections were stored in 0.1 M PB containing 0.05% sodium azide at 6 °C.

Adjacent free floating 40 μm sections were permeabilized in 0.4% Triton X-100 (TBS-T) for 30 min, blocked with 10% normal goat serum in TBS-T, and incubated for 65 h at 4 °C with polyclonal rabbit antibodies directed against RTN1A (1:2000; 2) or RyR 2 (1:2000; [16]). After three consecutive washes in TBS-T, the sections were incubated with HRP-coupled secondary antibody (P0448 goat anti-rabbit 1:500; DAKO, Glostrup, Denmark) in 10% blocking serum/TBS-T) for 2.5 h. Immunoreactions were visualized using 3,3′-diaminobenzidine tetrahydrochloride dihydrate (DAB, Sigma-Aldrich,Vienna, Austria). Sections were mounted on glass slides in 60% ethanol and allowed to dry overnight. After dehydration in ethanol and clearing in butyl acetate, they were coverslipped using Eukitt mounting medium. Controls included omission of the primary serum or its substitution by nonimmune rabbit serum, and no specific staining was visible on such preparations. In some experiments, RTN1A antibody solution has been pre-incubated with excess of recombinant RTN1A or RACK protein (10 μg/mL) at 4 °C overnight. Staining was absent in sections pretreated with such a solution (Suppl. Fig. 1). Analysis was performed under a Zeiss AxioPhot microscope equipped with Plan-Neofluar and Plan-Apo objective lenses (Zeiss, Vienna, Austria). Images were acquired with an AxioCam HR (Zeiss) controlled by the Openlab software (version 5.5.0; Improvision, Coventry, UK). For immunohistochemistry, sections for pre-embedding electron microscopy were incubated with the mouse monoclonal RTN1A MON162 antibody (diluted 1:250) and the antigen-antibody complex was visualized either by HRP or by nanogold-silver-enhanced reaction. Sections processed for the HRP reaction were incubated with biotinylated anti-mouse secondary antibodies (diluted 1:100; Vector Laboratories) and then in ABC complex (diluted 1:100; Vector Laboratories) made up in TB overnight at 6 °C. Visualization was carried out with DAB (0.5 mg/mL) using 0.003% H_2O_2 for 3–6 min. For the nanogold-silver-enhanced reaction, sections were incubated with Fab fragment secondary antibodies coupled to nanogold (1.4 nm, Nanoprobes Inc., Stony Brook, NY) and then extensively washed in milliQ water before silver enhancement of the gold particles with the HQ kit (Nanoprobes Inc.) for ~8–10 min. After both reactions, sections were subsequently washed with 0.1 M PB and treated with 2% OsO_4 in 0.1 M PB for 40 min at RT and contrasted with 1% uranyl-acetate in 50% ethanol for 30 min at RT. Sections were dehydrated and transferred into epoxy resin (Durcupan ACM, Sigma-Aldrich, Gillingham, UK) overnight at RT. The following day, the sections were transferred onto greased slides, coverslipped, and incubated for 3 days at 60 °C. Blocks of the cerebellar cortex were cut under a stereomicroscope and re-embedded in epoxy resin. Ultrathin sections (70 nm) were cut using a diamond knife (Diatome, Biel, Switzerland) on an ultramicrotome (Ultracut,

Vienna, Leica), collected on copper slot grids coated with pioloform and analyzed at 80 kV in a Philips CM120 electron microscope (Eindhoven, the Netherlands).

2.9. [^{3}H]Ryanodine Binding Assay

Preparation of purified rat forebrain synaptosomal membrane vesicles was described previously [29]. Equilibrium [^{3}H]ryanodine binding was essentially performed as described [30,31]. Briefly, 200 μg vesicles (12.5 μg/mL) were incubated at 0.5 M or 1 M KCl, 25 mM Pipes, pH 7.4 and varying free calcium concentrations, with 10 nM [^{3}H]ryanodine (American Radiolabeled Chemicals Inc., St. Louis, MO) for 2 h at 37 °C in the presence or absence of 0.1 μM GST-RTN$_{523}$ or 0.1 μM GST as control. Nonspecific binding was determined by measuring [^{3}H]ryanodine binding in the presence of 10 μM unlabeled ryanodine (Ascent Laboratories, UK). Bound [^{3}H]ryanodine was separated from free ligand by vacuum filtering through glass fiber filters (Whatman GF/C). Filters were washed 3 times with 5 mL each of ice-cold 10% binding buffer (0.1 M KCl, 2.5 mM Pipes, pH 7.4). Radioactivity was quantified by liquid scintillation counting. Specific binding was calculated as the difference between total and nonspecific binding measured in parallel assays. All binding assays were done in triplicates. Results shown are means +/− S.E.M. for n = 3–4 independent experiments. Statistical significance was evaluated using Student's *t*-test. [Free Ca^{2+} concentrations were calculated using MaxChelator software. (http://www.stanford.edu/~cpatton/maxc.html)].

3. Results

3.1. Identification of RyR2 as a binding partner of RTN1A

To better understand the function of neuronal RTN1A, we searched for protein-binding partners using pull-down experiments from mouse brain extracts with a GST-His-tagged fusion protein comprising aa 1–523 of rat RTN1A (GST-RTN1$_{523}$) (Fig. 1A). Specifically bound proteins were resolved by SDS-PAGE and visualized by Silver staining. One prominent band at high molecular weigth was consistently pulled down with varying amounts of the GST-RTN1$_{523}$ (Fig. 1A, *arrow*). This band was not seen in control lanes using GST, glutathione beads or GST-NiR, a recombinant fusion protein comprising aa 1–172 of rat reticulon protein NogoA/RTN-4A (Fig. 1A). We excised this band and subjected it to MS analysis, which identified 25 different peptides that belong to the cardiac RyR2, an ER-associated calcium-release channel, expressed in heart and brain (Suppl. Fig. 2; [32]). The association of GST-RTN1$_{523}$ and RyR2 was confirmed by Western blotting with an antibody specific for RyR2 (Fig. 1B). Two immunoreactive bands larger than 500 kDa, consistent with the size of RyR2, were detected. The higher molecular mass band corresponds most likely to intact RyR2, while the lower band presumably represents a proteolytic degradation fragment of RyR2. The intensity of the RyR2 bands increased proportionally with increasing amounts of GST-RTN1$_{523}$. Taken together, these results demonstrate that *in vitro* the RTN1A/RyR2 interaction was robust and concentration-dependent as GST-RTN1$_{523}$ was increased.

3.2. RTN1A associates with RyR2 in vitro and in vivo

To verify that RTN1A and RyR2 interact in a cellular system, we performed both *in vitro* and *in vivo* co-immunoprecipitation experiments. Full length myc-tagged RTN1A and untagged RyR2 were cotransfected into HEK293 cells, which lack endogenous expression of RTN1A or RyR2. As expected, RyR2 was readily co-immunoprecipitated with RTN1A (Fig. 2A), but not in the control experiments, when RyR2 was co-expressed with RTN4A-myc or if non-immune rabbit IgG was used as the precipitating antibody (Fig. 2A). Expression levels of RTN1A, RTN4A, and RyR2 were comparable between transfections as indicated by immunoblotting a fraction of the immunoprecipitation inputs (Fig. 2A). This shows that full length RTN1A can associate with RyR2 after heterologous expression in HEK293 cells.

Next we addressed if RyR2 and RTN1A interact under endogenous conditions in brain tissue. Because both RTN1A and RyR2 are expressed in the cerebellum [33,11] we employed reverse co-immunoprecipitation experiments using anti-RTN1A antibodies to precipitate RTN1A from rat cerebellar homogenate. Again, RyR2 was found to co-precipitate robustly with two different RTN1A antibodies. In contrast, RyR2 was not immunoprecipitated with non-immune IgG or two different anti-RTN4A antibodies, indicating the specificity of the co-immunoprecipitation (Fig. 2B,C). When RyR2 was immunoprecipitated using RyR2 specific antibodies, only RTN1A but not RTN4A was robustly precipitated with RyR2, again supporting a specific association of RTN1A and RyR2 (Fig. 2C). Moreover, RTN1A's *in vivo* interaction with RyR2 was isoform specific as it interacts with RyR2, but not with RyR1 (Fig. 2D) or InsP3R1, another ER-associated calcium release channel abundantly expressed in the cerebellum (Supp. Fig. 3; [33,34]). Our immunoblots also indicate that RTN1A associates with RTN4A, as rabbit anti-RTN1A antibodies co-precipitated RTN4A (Fig. 2B, lane 2). Similarly, RTN1A was weakly detected in immunoprecipitates with monoclonal anti-RTN4A antibodies (Fig. 2C, lane 4). This is in line with previous reports, showing that RTNs can form hetero-oligomers *via* their RHD domains [35,36].

Together, the results from these co-immunoprecipitation experiments suggest that RTN1A associates specifically with the RyR2 channel in the brain and possibly forms complexes composed of additional reticulon isoforms.

3.3. RyR2-dependent redistribution of RTN1$_{523}$ in HEK293 cells

As an independent verification of the data, we expressed mCherry-RTN1$_{523}$, alone or in the presence of the RyR2 receptor in HEK293 cells, and examined the subcellular distribution of the RTN1$_{523}$ construct. Expression of mCherry-RTN1$_{523}$ lacking the RHD displayed a diffuse distribution in the cytoplasm (Fig. 3A, a), confirming that the RHD of reticulons plays a role in targeting and stabilization of the proteins in the ER membrane [37,38]. In comparison, immunocytochemical stainings of cells single-transfected with untagged RyR2 or RyR1 revealed a well defined and typical staining pattern of ER targeted proteins with a highly organized web-like distribution throughout the cell (Fig. 3A,b–c).

Double immunofluorescence staining confirmed that both RyR isoform proteins are localized to the ER as evidenced by the strong colocalization of their staining with calreticulin, an endogenous ER marker (Fig. 3B). Interestingly, co-expression of mCherry-RTN1$_{523}$ with RyR2 resulted in a partial redistribution of RTN1$_{523}$ from cytosolic to ER location, overlapping with RyR2 in the perinuclear region as well as tubular network (Fig. 3A, d–f). Notably, the redistribution of RTN1$_{523}$ was specifically dependent on its interaction with RyR2, as RTN1$_{523}$ maintained a diffuse localization in the cytosol when it was co-expressed with RyR1 (Fig. 3A, g–i), that was unable to bind RTN1A (Fig. 2D). As a result, the rate of colocalization as quantified by using the Pearson's correlation coefficient was much higher between RTN1A$_{523}$ and RyR2 (Pearson's coefficient = 0.76 ± 0.10) than between RTN1A$_{523}$ and RyR1 (Pearson´s coefficient = 0.28 ± 0.09; $p = 0.003$) (Fig. 3C). Thus, the colocalization between RTN1$_{523}$ and RyR2 supports a highly specific direct interaction of both proteins.

3.4. RyR2 binds to a conserved domain in the N-terminal region of RTN1A

To define more specifically the RyR2 binding region within RTN1A, we generated two non-overlapping sub-fragments of RTN1$_{523}$ (long N-terminal fragment, LNT, aa 1–375; high homology domain, HHD, aa 376–523; Fig. 4A) and performed GST pull-down assays on mouse brain lysates. As shown in Fig. 4B, RyR2 specifically interacted with GST-RTN1$_{523}$ and GST-HHD, but not with GST-LNT or the negative controls (Fig. 4B, *upper panel*). These data indicate that the HHD domain, aa

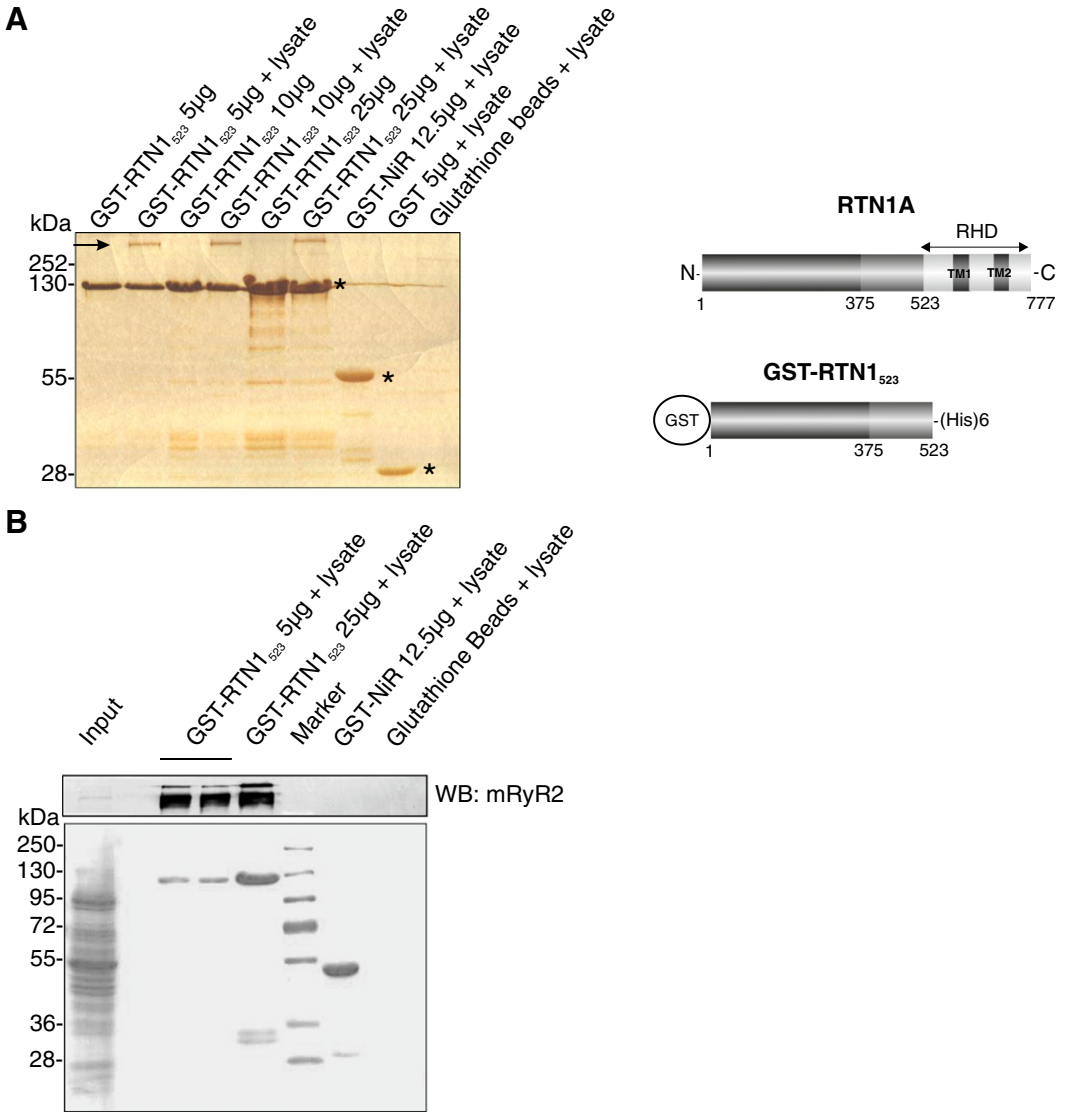

Fig. 1. Identification of RyR2 as a binding partner of RTN1A. (A) Schematic representation of full length RTN1A and the GST-RTN1$_{523}$ construct (*right*). RHD: reticulon homology domain; TM1 and TM2: transmembrane domain 1 and 2. GST pull-downs were performed with GST-RTN1$_{523}$ using detergent-solubilized mouse brain proteins. GST or empty glutathione beads served as negative controls, whereas GST-NiR was tested to control for GST-RTN1$_{523}$ binding specificity. Arrow denotes protein band that was consistently pulled down with GST-RTN1$_{523}$ and from which RyR2 was identified by mass spectrometry. Note that this band is absent in the different control samples. Asterisks indicate the GST fusion proteins and their relative amounts used in the GST pull-down. The silver stained gel shown is representative of three independent experiments. (B) *Upper panel*, Western Blot of samples from (A) probed with RyR2 antibody. Note the double-band that is identified as RyR2. The higher molecular mass band corresponds to intact RyR2, while the lower band presumably represents a proteolytic degradation fragment of RyR2. The intensity of the RyR2 bands increase with increasing amounts of GST-RTN1$_{523}$. *Lower panel*, shows Ponceau S staining of the pull-downs to assess the relative amounts of each GST fusion protein. Input lane shows one-twentieth of the amount used for pull-down. WB, Western blot. The Western blot shown is representative of three independent experiments.

376–523 of RTN1A, contains the binding site(s) for RyR2 *in vitro*. Interestingly, this region was found to display significant sequence homology from human to Xenopus, (thus we termed this region high homology domain, HHD), suggesting that this domain was highly conserved over evolution.

3.5. RTN1A displays an overlapping expression pattern with RyR2 in brain

RTN1A and RyR2 have been both reported to be expressed in brain [11,12,39–41]. Because our GST fusion protein affinity pull-down and co-immunoprecipitation experiments from total brain or cerebellar extracts provide biochemical evidence for the association of RTN1A and RyR2 in a complex, we predicted that their expression patterns would overlap. To address this hypothesis, we examined the distribution of RyR2 and RTN1A in different regions and cell types of the brain using immunohistochemical analysis on adult rat brain sections. Indeed, RTN1A and RyR2 were found to be codistributed in many brain regions, although their staining pattern was not identical. The highest immunoreactivity of both RTN1A and RyR2 was in the hippocampus and cerebellar Purkinje neurons (Fig. 5). In line with a previous study, RyR2 displayed intense immunoreactivity in the molecular layer of the dentate gyrus as well as in mossy fibers and stratum lucidum, a region of high synaptic plasticity where mossy fibers synapse with CA3 pyramidal cell apical dendrites (Fig. 5B; [40]). A similar staining pattern was found for RTN1A (Fig. 5A), revealing strong expression in mossy fibers and stratum lucidum. In the adult rat cerebellum, two independent anti-RTN1A antibodies revealed a strong immunoreactivity in Purkinje cell somata, axons and dendrites whereas cerebellar interneurons, Bergman glia and granule cells remained unlabeled (Fig. 5C, D). Consistent with previous reports, immunofluorescent RyR2 specific staining was predominantly found in granule cells, and more moderatly in Purkinje cell somata and

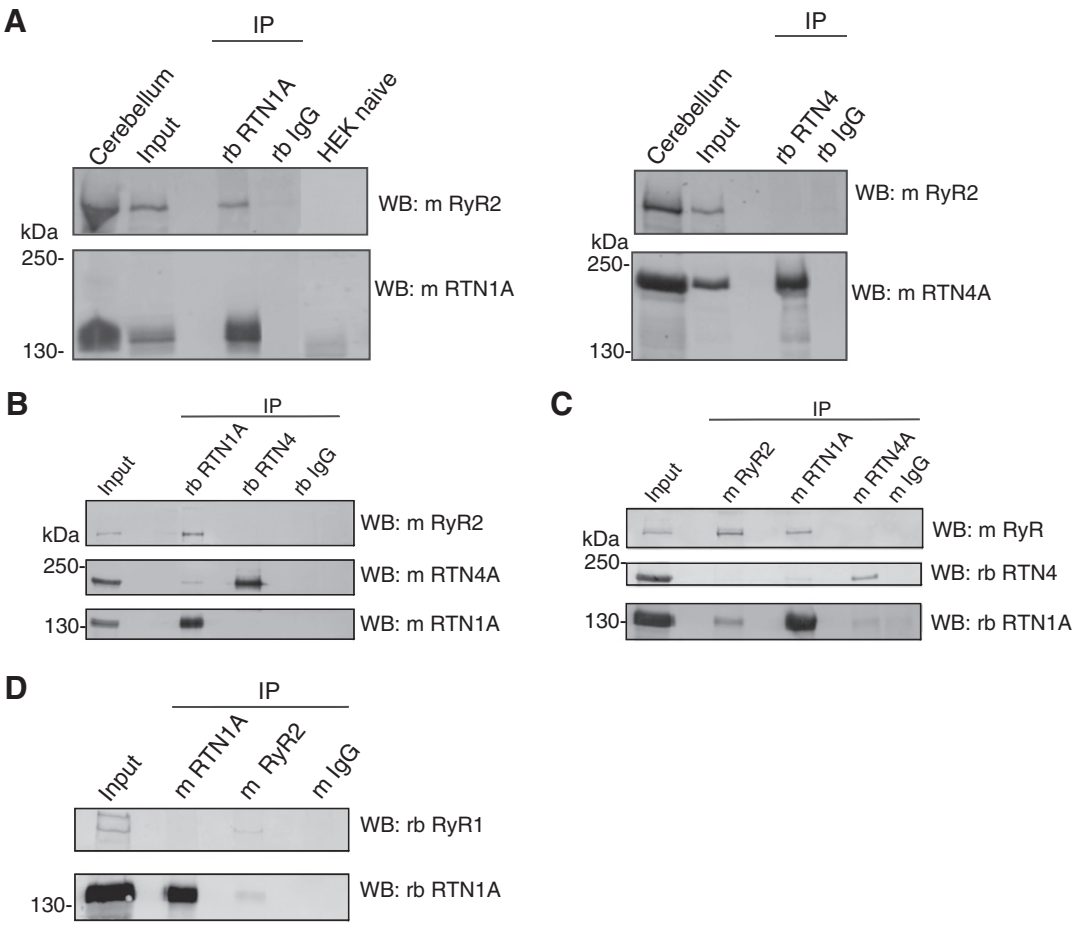

Fig. 2. RTN1A associates preferentially with RyR2 channel *in vivo*. (A) *Left panels*, detergent-solubilized protein from HEK293 cells transiently transfected with untagged RyR2 plus RTN1A-myc was immunoprecipitated (IP) with rabbit polyclonal anti-RTN1A antibodies or control rabbit IgG. Immunoprecipitated proteins were detected on immunoblots with monoclonal anti-RyR2 or anti-RTN1A antibodies. Note that native HEK293 cells do not express endogenous levels of RTN1A or RyR2. *Right panels*, detergent-solubilized protein from HEK293 cells transiently transfected with untagged RyR2 plus RTN4A-myc was immunoprecipitated with rabbit polyclonal anti-RTN4 antibodies or control rabbit IgG. Immunoprecipitated proteins were detected on immunoblots with monoclonal anti-RyR2 or anti-RTN4A antibodies. Input lane shows one-eighth of the amount used for immunoprecipitation. WB, Western blot. (B) Detergent-solubilized protein from rat cerebellum was used for co-immunoprecipitations with rabbit anti-RTN1A, rabbit anti-RTN1A, or control rabbit IgG. Immunoprecipitated proteins were resolved by SDS-PAGE blotted on PVDF membranes and probed with monoclonal antibodies as indicated at the right. Input lane shows one-tenth of the amount used for immunoprecipitation. WB, Western blot. (C) Detergent-solubilized protein from rat cerebellum was used for co-immunoprecipitations with mouse anti-RyR2, mouse anti-RTN1A, mouse anti-RTN1A, or control mouse IgG. Immunoprecipitated proteins were resolved by SDS-PAGE, blotted on PVDF membranes and probed with antibodies as indicated at the right. Input lane shows one-tenth of the amount used for immunoprecipitation. WB, Western blot. (D) Detergent-solubilized protein from rat cerebellum was immunoprecipitated with mouse anti-RTN1A, mouse anti-RyR2, or control mouse IgG. Immunoprecipitated proteins were resolved by SDS-PAGE, blotted on PVDF membranes and probed with antibodies as indicated at the right. Note that RyR1 co-immunoprecipitates with mouse anti-RyR2, but not with mouse anti-RTN1A antibodies. Input lane shows one-fifth of the amount used for immunoprecipitation. WB, Western blot.

dendrites (Fig. 5E; [40]). Unfortunately, our attempts to reveal double immunofluorescent staining for RTN1A and RyR2 showed somewhat variable results due to inconsistency with the monoclonal RyR2 antibody.

3.6. Subcellular localization of RTN1A by immuno EM

Next, to resolve the precise subcellular distribution of RTN1A in Purkinje cells, we carried out pre-embedding immunoelectron microscopy visualizing the antigen-antibody complex either by means of the HRP-DAB reaction, because of the higher sensitivity, or by silver-enhanced nanogold reaction, which allows a more confined localization of the complex. In the molecular layer, the electron opaque peroxidase end product was observed in Purkinje cell dendrites and dendritic spines in apparent association with cisternal organelles and membranes of the smooth endoplasmic reticulum (Fig. 6A–B). On the other hand, other organelles such as mitochondria, lysosomes and multivesicular bodies, as well as the plasma membrane were unlabeled (Fig. 6A–B). Likewise, in parallel fiber axons and boutons, in axon terminals forming symmetric synapses and in glial processes we could not detect any RTN1A-IR. The silver-enhanced immunogold reaction confirmed that in the somatodendritic domain of Purkinje cells RTN1A-IR was exclusively intracellular. Immunometal particles decorated cisterns and vesicles of the smooth ER in Purkinje cell dendrites (Fig. 6C) and spines (Fig. 6D).

3.7. GST-RTN1$_{523}$ causes a decrease in [^{3}H]ryanodine-binding

To assess the functional impact of RTN1A interaction on the RyR2 Ca^{2+}-release channel, we performed equilibrium [^{3}H]ryanodine-binding assays on rat brain synaptosomes. Because ryanodine binds only to the open conformation of RyR this assay is considered a reliable measure of the open/closed state of RyR channels [42]. We determined the calcium dependence of [^{3}H]ryanodine binding to the population of RyR channels present in synaptosomes from rat brain in the presence or absence of RTN1A (purified GST-RTN1$_{523}$ at 0.1 μM). In line with previous studies for brain RyRs [43–48] our determinations showed that [^{3}H]ryanodine binding was similar to background levels in the virtual absence of [Ca^{2+}], reflecting the closed state of RyR channels, but was increased at higher [Ca^{2+}], with a characteristic "bell-shaped" [Ca^{2+}] dependence

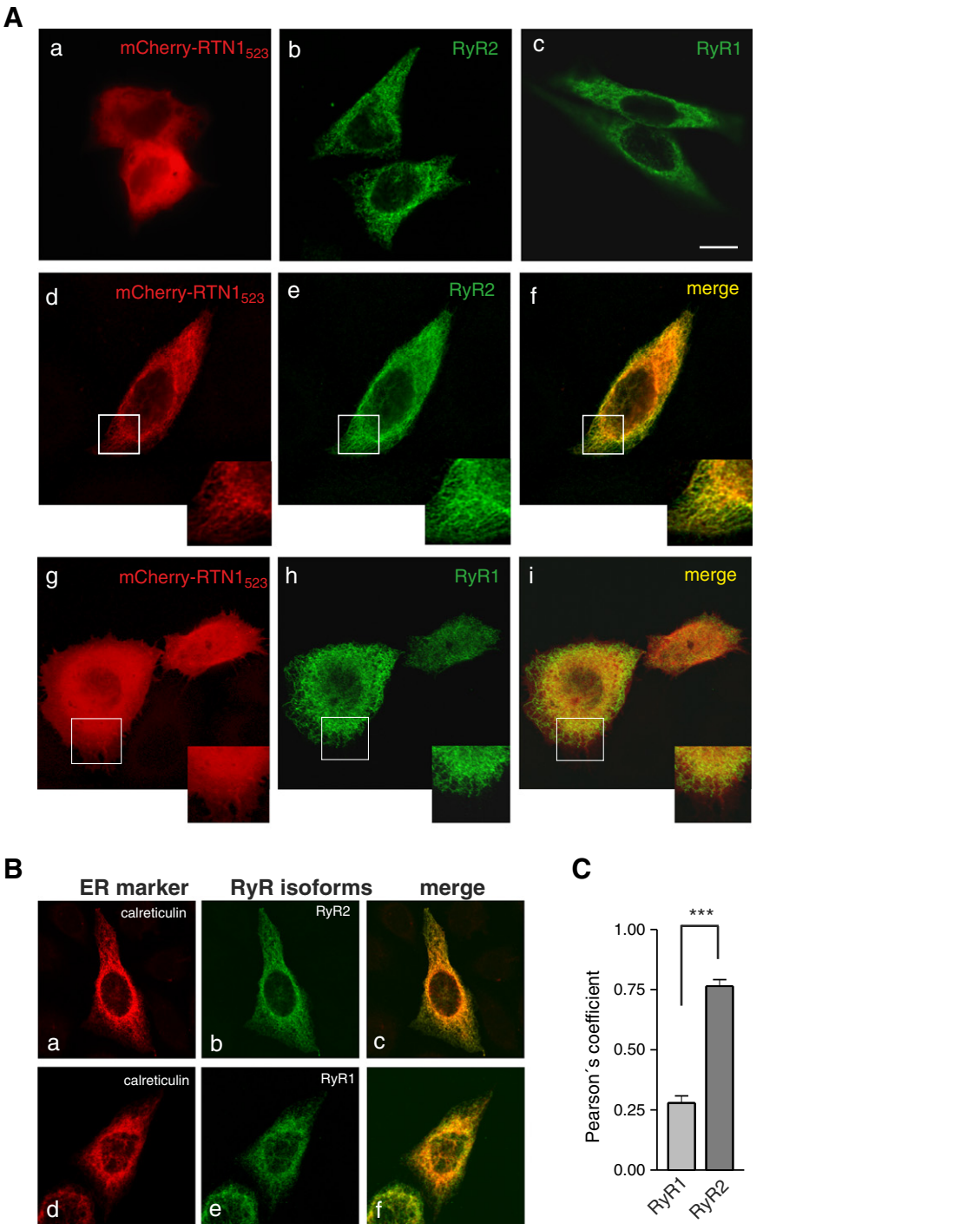

Fig. 3. Immunocytochemical distribution of mCherry-RTN1$_{523}$ and RyRs in HEK293 cells. (A) HEK293 cells were transiently transfected with mCherry-RTN1$_{523}$ in the absence (a) or presence of untagged RyR2 (d–f) or RyR1 (g–i). Single-transfections of untagged RyR2 (b) and RyR1 (c) were carried out as a comparison. Cells were immunostained with anti-RyR2 (b,d–f) or anti-RyR1 (c,g-i) antibodies and visualized by confocal microscopy. Note that single-transfected mCherry-RTN1$_{523}$ is uniformly distributed in the cytosol (a), but altered to a more reticular staining pattern when co-expressed with RyR2 (d–f). mCherry-RTN1$_{523}$ remained uniformly distributed in cells cotransfected with RyR1 (g–i). Cells shown represent at least 20 representative cells per condition. (B) Immunofluorescence confocal microscopy analysis of RyR ER localization in HEK293 cells. HEK293 cells were single-transfected with untagged RyR1 cDNA or RyR2 cDNA, immunostained with the indicated antibodies and imaged using immunofluorescence microscopy to demonstrate RyR and calreticulin (ER-specific marker) colocalization. Cells were immunostained for RyR isoforms (green) and Calreticulin (red), respectively. Space bar: 10 μm. (C) Extent of colocalization between mCherry-RTN1$_{523}$ and RyR isoforms was quantified using Pearson correlation coefficient and determined through correlation analysis with Leica SP5 software from 10 different cells per group. (***$p = 0.003$ by Student's *t*-test).

(Fig. 7A). Maximal activation of [^{3}H]ryanodine binding occurred between 1 and 10 μM Ca^{2+}, which is in agreement with previous studies [42–46]. Addition of 0.1 μM recombinant GST-RTN1$_{523}$ specifically reduced [^{3}H] ryanodine binding to synaptosomes at all calcium concentrations (Fig. 7A) without a major change in the profile of Ca^{2+} dependence. The presence of GST-RTN1$_{523}$ did not change the minimal [Ca^{2+}] for RyR activation (>10 nM Ca^{2+}), and maximal activity of RyRs was reached at the same [Ca^{2+}] as in the absence of GST-RTN$_{523}$. To compare the results obtained with different vesicle preparations, binding was normalized against the value determined in the absence of recombinant proteins. As shown in Fig. 7B, at 0.3 μM [Ca^{2+}], GST-RTN1$_{523}$ specifically inhibited [^{3}H]ryanodine binding to synaptosomes by

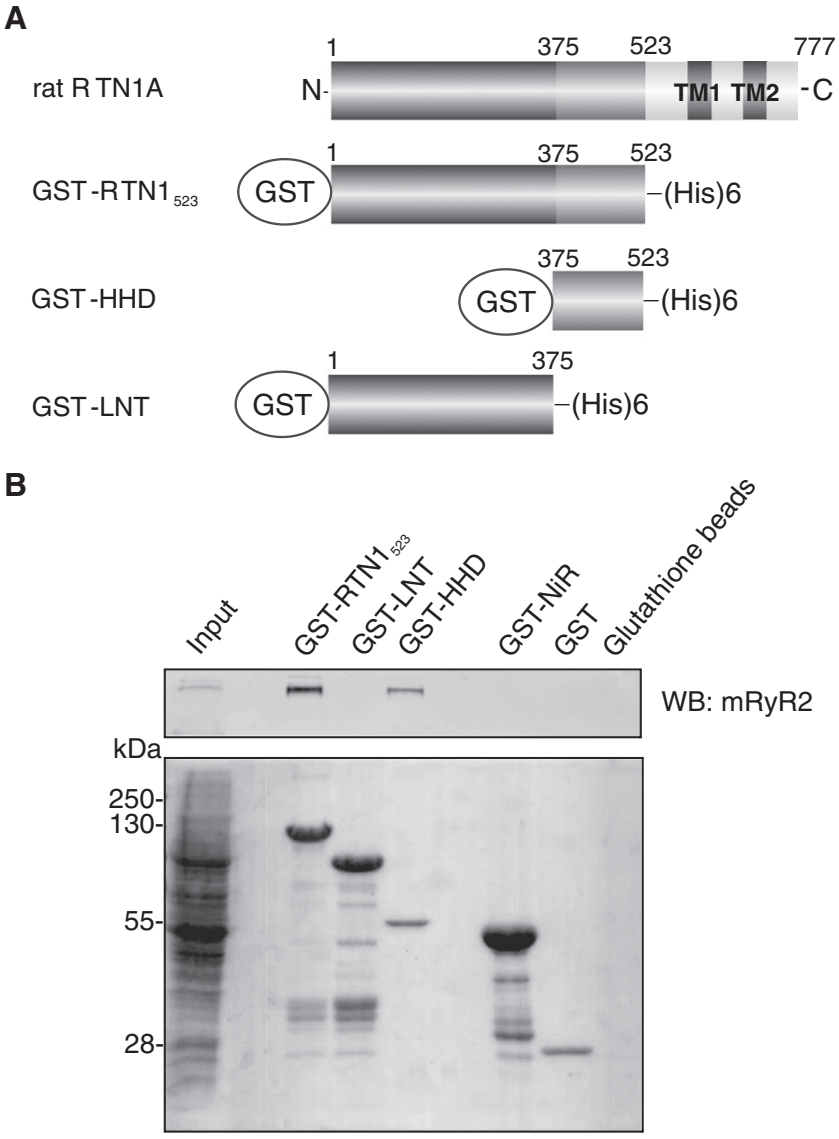

Fig. 4. Identification of the RyR2 binding domain. (A) Schematic representation of rat RTN1A protein and RTN1A fragments used to construct GST fusion proteins for the pull-down experiments. HHD: high homology domain; LNT: long N-terminal fragment. (B) GST-RTN1 fragments were used as baits in pull-down experiments using detergent-solubilized mouse brain proteins. GST, GST-NiR or empty glutathione beads served as negative controls. Binding of RyR2 was subsequently detected by immunoblot (*upper panel*). Ponceau S staining of the pull-downs shows the relative amounts of each GST fusion protein (*lower panel*). Input lane shows one-tenth of the amount used for immunoprecipitation. WB, Western blot. Results are representative of three independent experiments.

31.5 ± 4.3% compared to control conditions (n = 3; $p = 0.011$). This effect is entirely attributable to recombinant GST-RTN1$_{523}$ since 0.1 μM GST had no significant effect (1.4 ± 5.3%) in three parallel experiments. This downward shift in the [^{3}H]-ryanodine binding produced by RTN1$_{523}$, indicated a decreased Ca^{2+}-induced activation of RyR compared with control and is indicative of a decrease in RyR channel activity, since ryanodine binding increases as RyR activity increases.

3.8. RTN1A reduces RyR2-mediated Ca^{2+} oscillations

Ca^{2+} oscillations mediated by RyR2-expressing HEK293 cells at increased extracellular calcium concentrations were taken as a sensitive measure to detect an effect of RTN1A on RyR2 activity. As shown in Fig. 7C, Ca^{2+} transients were monitored in individual HEK293 cells expressing RyR2 in the absence or presence of RTN1A. To elicit maximal amount of RyR2-mediated Ca^{2+} oscillations, cells were perfused with 1 mM [Ca^{2+}]. By a quantitative analysis based on the overall area under the oscillations peaks during 450 s, the amount of Ca^{2+}-released *via* RyR2 was significantly reduced when mcherry-RTN1A was co-expressed in comparison to control with mcherry (Fig. 7C, left and right upper panel, right lower panel). Furthermore, the number of Ca^{2+} oscillating HEK293 cells (87.1%) was clearly reduced in the presence of RTN1A (51.9%) (Fig. 7C; right lower panel). In order to evaluate non RTNA1-specific ER-mediated effects on RyR2, we utilized RTN4A as an ER-resident control protein that did not interact with RyR2 based on our co-immunoprecipitation studies. Although co-expression of RTN4A with RyR2 slightly decreased the amount of Ca^{2+} released *via* RyR2, this effect was not significant (Fig. 7C; left lower panel). Additionally, the percent of HEK293 cells that developed RyR2-mediated Ca^{2+} oscillations (74.6%) was clearly above those with RTN1A co-expressed. The magnitude of Ca^{2+} released during 10 mM caffeine exposure was not substantially altered when RyR2 was co-expressed with either RTN1A or RTN4A (Fig. 7C; right lower panel). Together, these results suggest that a functional role for the association of RTN1A with RyR2 in neurons

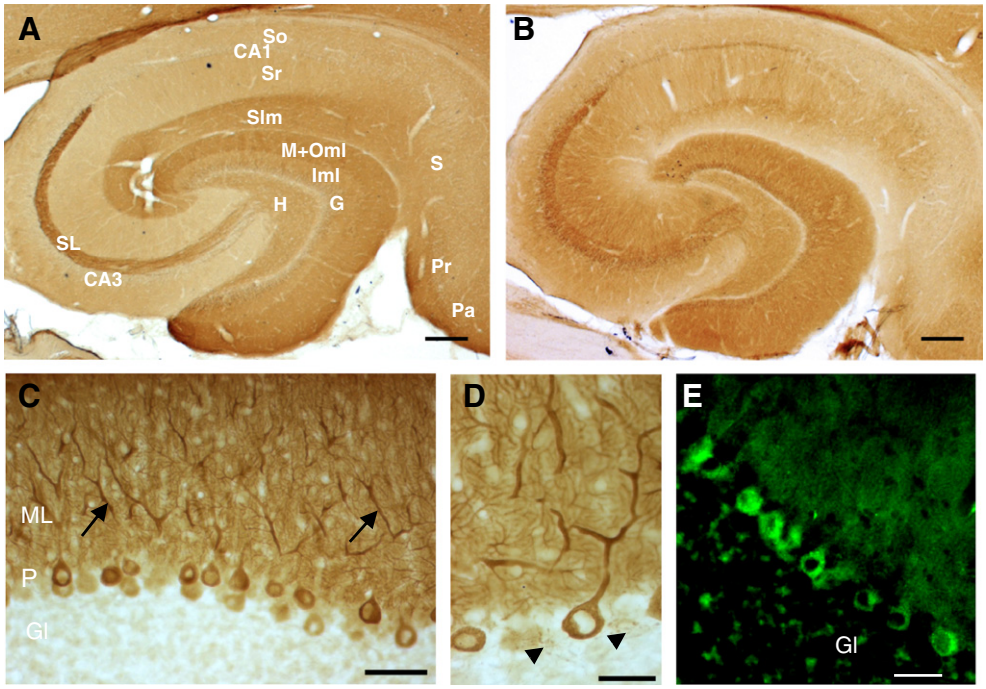

Fig. 5. Immunohistochemical distribution pattern of RTN1A and RyR2 in rat hippocampus and cerebellum. Representative staining patterns for RTN1A (A,C,D) and RyR2 (B,E) on sections of rat hippocampus (A,B) and cerebellar cortex (C,D,E). In the hippocampus, immunoreactivity for both proteins is found in granule cells (G), mossy fiber axons, and in stratum lucidum (SL). In the cerebellum, RTN1A-immunoreactivity was confined to Purkinje cell bodies (P), their dendrites in ML (C; arrow) and axons (D; arrowheads). (E) Confocal immunofluorescent image showing RyR2 staining in Purkinje cells. Unlike RTN1A, RyR2 was also found in granule cell layer (Gl). Scale bars: A and B, 500 μm; H, hilus; G, Granule cell layer; So, stratum oriens; Sr, stratum radiatum; Slm, stratum lacunosum molecular; Iml, inner molecular layer; M + Oml, Middle & outer molecular layer; CA1-3, Cornu ammonis; SL, stratum lucidum; S, Subiculum; Pr, Presubiculum; Pa, Parasubiculum.

is in the regulation of intracellular calcium dynamics of pre- and post-synaptic calcium stores.

4. Discussion

Despite the abundant expression of RTN1A in the adult brain, our understanding of its functional role still remains elusive. In this study, using a combination of co-immunoprecipitation, colocalization, GST pull-down assays and MS analysis we identify the intracellular calcium release channel RyR2 as a RTN1A binding partner in neurons. Moreover, we show that soluble $RTN1_{523}$ reduces Ca^{2+}-induced activation of RyR on brain synaptosomes and that RTN1A markedly decreases the occurrence of RyR2-mediated Ca^{2+} oscillations at elevated extracellular Ca^{2+} concentrations.

4.1. Interaction of RTN1A and RyR2

In our study we provide evidence for a direct interaction of RTN1A and RyR2. Several approaches were used to confirm this finding. First, different RTN1A antibodies immunoprecipitated RyR2 after heterologous expression in HEK293 cells and from detergent-solubilized brain extract. This interaction was not seen with precipitating RTN4A/NogoA antibodies. Second, cytosolic mCherry-$RTN1_{523}$ relocalized when co-expressed with RyR2 but not with RyR1 in HEK293 cells. Third, GST-$RTN1_{523}$ affinity beads were shown to pull-down RyR2 but not RyR1 from detergent-solubilized brain extract. Thus, it seems that both proteins form a functional complex in neurons, although we cannot completely exclude the possibility that the two proteins may indirectly interact by virtue of each binding to an intermediary protein.

Previous studies in non-neuronal cells have suggested that all reticulons including RTN1A partition into the outer leaflet of the ER membrane bilayer *via* their RHD, placing the N-terminal and C-terminal domains in the cytoplasm [37,38,49,50]. Since we used the N-terminal domain of RTN1A (aa 1–523) for interaction analysis we propose that in intact cells RTN1A–RyR2 interaction occurs from the cytosolic surface from the ER membrane *via* cytosolic domains. More specifically, the principal region of RTN1A responsible for binding RyR2 was mapped to HHD, the portion of the protein spanning amino acid residues 376 and 523 (Fig. 4). No binding was detected within the N-terminal half of the protein between residues 1 and 375. Strikingly, this RyR2 binding region of RTN1A is highly conserved among all RTN1A and RTN1B isoforms that have so far been characterized from different species including African clawed frog (*Xenopus laevis*), chicken (*Gallus gallus*), Carolina anole (*Anolis carolinensis*), gray short-tailed opossum (*Monodelphis domestica*), platypus (*Ornithorhynchus anatinus*), house mouse (*Mus musculus*), Norwegian rat, (*Rattus norvegicus*), Cattle (*Bos taurus*), and man (*Homo sapiens*), suggesting a central role for the HHD region in the function of these two proteins. An unexpected finding from this study is the preferential interaction of RTN1A to RyR2 relative to RyR1. The similarities in protein structure and subcellular localization between both RyRs led us to investigate whether RyR1, like RyR2, is capable of binding to RTN1A. Although our present biochemical analysis did not detect a RyR1 association with RTN1A (Figs. 2D and 3), we cannot exclude that both proteins may associate weakly/transiently, or alternatively, that only minor amounts of these proteins interact in specific neurons. Nevertheless, this selectivity could reflect preferential binding of RTN1A to RyR2 in the absence of RyR1 such as in hippocampal mossy fibers (see below). Interestingly, in muscle cells, the two FK506-binding proteins (FKBPs), FKBP12 and FKBP12.6, also known as immunophilins, also exhibit selectivity binding to certain RyR subtypes. While FKBP12 can potentially regulate all three RyR subtypes, with a selectivity of RyR1 > RyR3 > RyR2 [51,52], FKBP12.6 associates preferentially with RyR2 [53] and regulates RyR2 mediated Ca^{2+} release by stabilizing the channel in its closed state [54]. Future studies will need

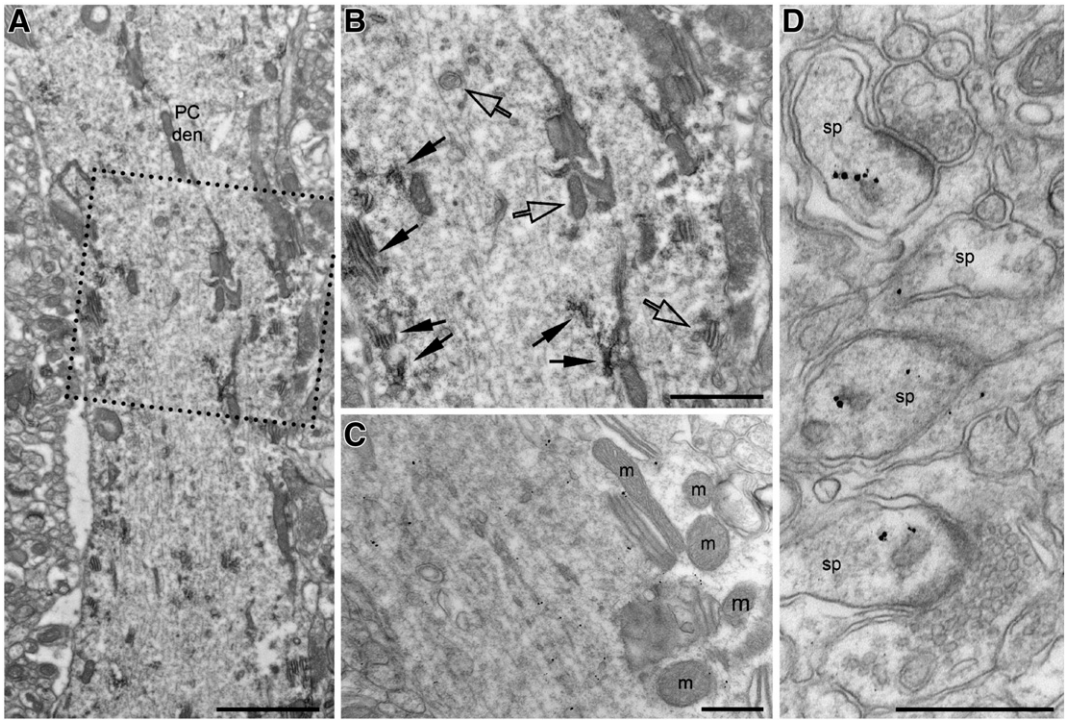

Fig. 6. Subcellular distribution of RTN1A in Purkinje cells. (A) Electron micrograph of a Purkinje cell dendrite immunolabeled for RTN1A (MON162 antibody) using the HRP-DAB technique. (B) Higher magnification of the area boxed in A. The electron opaque peroxidase end product can be seen around cisternal organelles and vesicles of the smooth endoplasmic reticulum (indicated by filled arrows), but not the plasma membrane of the Purkinje cell. Empty arrows indicate unlabeled organelles. (C) Electron micrograph of a Purkinje cell dendrite immunolabeled for RTN1A (MON162 antibody) using the silver-enhanced nanogold technique. Immunometal particles can be seen decorating the membrane of cisternal organelles and vesicles of the smooth endoplasmic reticulum but not the mitochondria (m). (D) Immunometal particles for RTN1A can be observed associated with the smooth endoplasmic reticulum within Purkinje cell spines (sp). Scale bars: A, 2 μm; B, 1 μm; C–D, 500 nm.

to explore the potential for RyR subtype-specific interactions with other RTN isoforms.

4.2. Expression and subcellular localization of RTN1A in neurons

Thus far, little information is available for detailed subcellular localization of different RTN isoforms. Here, we explored the cellular and subcellular distribution of RTN1A in detail. Immunohistochemical studies revealed an intense labeling of RTN1A in mossy fibers of the hippocampus as well as in axons, dendrites and spines of Purkinje cells. Immunoelectron microscopy clearly showed that RTN1A was highly enriched in dendrites and spines, and mostly distributed around the smooth ER. Although RTNs are generally thought to be predominantly located in the endomembrane system, RTN4A, -B, -C and RTN2B were reported to reside also on the cell surface of neurons and non-neuronal cells [55,56,36,4]. In contrast, in our immunoelectron microscopy study we did not observe plasma membrane associated RTN1A-IR in Purkinje cells (Fig. 6). This finding is in perfect agreement with previous cell surface biotinylation assays on cultured neurons, which failed to detect cell surface-exposed RTN1A [4]. Moreover, in contrast to the RHD of RTN2, -3 and −4 proteins, RHD of RTN1 lacks binding to the axonal Nogo-66 receptor, NgR1 [57] thought to be responsible for axonal growth inhibition. Hence, it seems likely that RTN1A exerts primarily an intracellular function related to its localization within the ER of pre- and postsynaptic sites. Although RTN1A shows a similar distribution in the brain as the RyR2 channel, it also exhibits a distinct expression pattern compared to RyR2 when examined in detail locally. For example, both proteins are highly expressed in cerebellum; however, RTN1A is more abundant in Purkinje cells whereas RyR2-IR is strong in granule cells, which are clearly devoid of RTN1A-IR, implying that RTN1A/RyR2 association may play distinct roles in subregions of the cerebellum.

4.3. Physiological function of RTN1A–RyR2 association

At present, the physiological significance of the RTN1A–RyR2 association remains to be defined. However, it is tempting to speculate that RTN1A might exert a regulatory effect on RyR2 channel function. Initial evidence for a modulatory role of RTN1A is provided by our ryanodine binding assays, showing that soluble $RTN1_{523}$ inhibits the calcium-dependent activation of [^{3}H]ryanodine binding in forebrain synaptosomes by 32% (Fig. 7A,B). Because RyR2 was shown to be the most abundant isoform of total RyR content in mammalian brain cortex [58,41], we assume that this decrease in [^{3}H]ryanodine binding is largely attributable to $RTN1_{523}$ association to RyR2. Consistent with this view, we have shown that RTN1A reduces the frequency of RyR2-mediated Ca^{2+} oscillations in HEK293 cells expressing RyR2. Although this effect appeared to be specific for RTN1A, we cannot fully exclude that overexpression of RTN1A in the ER additionally contributed to its specific inhibitory action on RyR2 function. Hence, the apparent close physical proximity of the RyR2 and RTN1A in Purkinje cells or in mossy fibers in the hippocampus (Fig. 5) may enable RTN1A to bind to the RyR2 channel with high avidity even when cytoplasmic Ca^{2+} concentration is low under resting conditions. Accordingly, RyR2 channels that are bound to RTN1A may have a lower open probability, resulting in a decreased sensitivity to RyR2-mediated CICR. Emerging evidence indicates that CICR appears to play a vital role in neuronal functions including those that regulate synaptic efficacy, aging and memory. CICR has been demonstrated in neurons where intracellular Ca^{2+} release from RyRs is found to be linked to Ca^{2+} influx through voltage-dependent channels [59]. In cerebellar Purkinje cells, for example, Ca^{2+} influx *via* activation of both ionotropic and metabotropic glutamate receptors is shown to be essential for subsequent RyR-mediated Ca^{2+} release [60]. In addition, RyR mediated Ca^{2+} release from intracellular stores is reported to

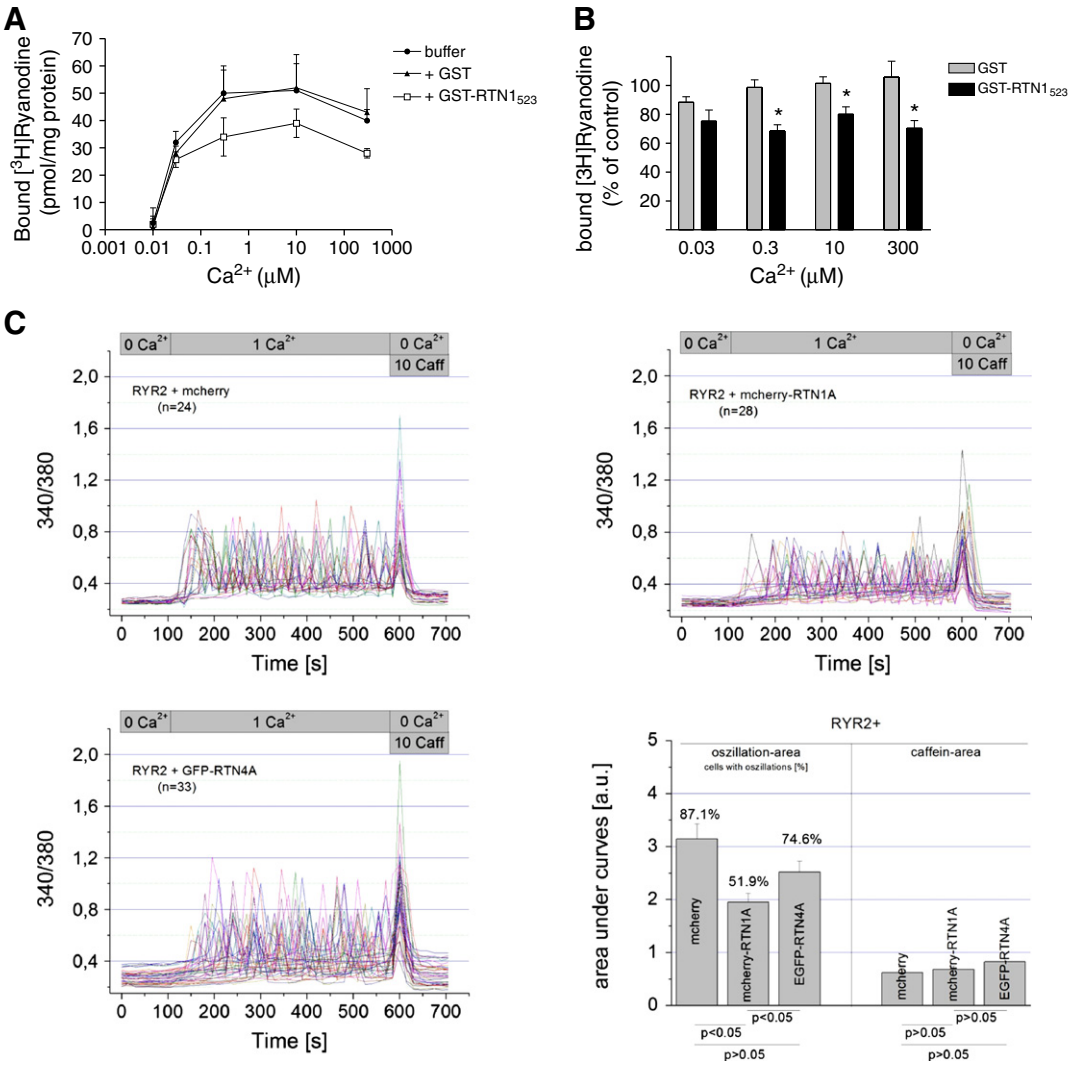

Fig. 7. GST-RTN1$_{523}$ inhibits specific [^{3}H]ryanodine binding to rat brain synaptosomes. (A) Equilibrium [^{3}H]ryanodine binding to rat forebrain synaptosomal membrane preparations was carried out in binding buffer containing 10 nM [^{3}H]ryanodine at the indicated free calcium concentrations in control conditions (*closed circles*) and in the presence of 0.1 μM GST (*closed triangles*) or 0.1 μM GST-RTN1$_{523}$ (*open squares*). [Ca^{2+}] was maintained, in the range 0.01 μM–1 mM, by a combination of EGTA and $CaCl_2$. Free Ca^{2+} concentrations were calculated as described in material and methods. Data points shown are the mean ± S.E.M., from three separate experiments performed in triplicates. (B) [^{3}H]ryanodine binding in the presence of 0.1 μM GST or GST-RTN1$_{523}$ is presented as percent of control. No specific [^{3}H]ryanodine binding was observed at 0.01 μM Ca^{2+} in the presence of GST or GST-RTN1$_{523}$. Difference in [^{3}H]ryanodine binding was plotted as percent decrease in specific binding. Data points shown are the mean ± S.E.M., from three separate experiments (*$p = 0.011$ by Student's *t*-test). (C) RyR2 evoked Ca^{2+} oscillations in HEK293. *Upper and lower left panels* represent Fura-2 ratio time-courses of single cells expressing RyR2 together with mcherry, mcherry-RTN1A or EGFP-RTN4A. Cells were continuously perfused with buffer containing 0 mM Ca^{2+} (nominal free), 1 mM Ca^{2+} and 0 mM Ca^{2+} + 10 mM caffeine as indicated by the bars at the top. Lower right panel shows a quantitative analysis performed by integration of the respective single peak areas referred to *area under curve* for estimation of the total amount of the cytosolic [Ca^{2+}] arising through RyR2 dependent Ca^{2+} oscillations. The fraction of cells that showed both oscillations as well as a clear caffeine peak in comparison to those that lacked oscillations before a single caffeine peak are given in percentages in the graph. A two-sample *t-test* was carried out to test for significance as indicated by the *p* values at the bottom of the panel.

be required for induction of long-term potentiation in the hippocampus [61,62] and long-term depression in both the hippocampus and cerebellum [63–66]. Notably, in the hippocampus, activity dependent presynaptic CICR at the mossy fiber synapse is mediated by RyR2 [40], thereby facilitating robust presynaptic forms of plasticity at the mossy fiber-CA3 synapse. Hippocampal expression of RyR2 increases after spatial memory learning [63] and is involved in BDNF-induced hippocampal synaptic plasticity and spatial memory formation [67].

The RTN1A and RyR2 association might not only be involved in neurotransmitter release but also in aging-related Ca^{2+} dysregulation. Similar as in the muscle (see above), neuronal FKBP12.6 inhibits cytosolic Ca^{2+} rises by inhibiting directly L-VGCCs and RyR2. Interestingly, experimental silencing or downregulation of FKBP12.6, led to hippocampal Ca^{2+} dysregulation resulting in dampened neuronal excitability and function, typical signs of aging or pathological neurons [68]. Thus, in analogy, it is possible to envision that, in neurons, RTN1A may function together with RyR2 and FKBP molecules in a multimeric Ca^{2+} regulating complex, in which RTN1A and FKBP12.6 tonically inhibit RyR2 by direct interaction.

In conclusion, we identified RyR2 as a novel binding partner of RTN1A and show that RTN1A exerts a regulatory, inhibitory effect on the RyR2 activity. These results suggest that a functional coupling of RTN1A and RyR2 may play a vital role in controlling regulation of neurotransmitter release and long-term potentiation induction by modulation of intracellular Ca^{2+} release.

Supplementary data to this article can be found online at http://dx.doi.org/10.1016/j.bbamcr.2013.02.012.

Acknowledgements

We thank P.D. Allen and Wayne Chen for generously providing rabbit RyR1 and mouse RyR2 cDNA constructs, and Vincenzo Sorrentino for the polyclonal anti-RyR2 antibody. We are very grateful to Sabrina Riepler, Antje Kurz and Gabi Schmid for excellent technical assistance, Gerald Obermair for advice on statistical analysis, Martin Offterdinger for help on colocalization studies and the SPIN consortium for critical discussions. This work was supported by the Austrian Research Foundation (FWF W1206) and an IFTZ-grant to CEB. LK was supported by the Graduate program 'Signal processing in neurons' (SPIN).

References

[1] Y.S. Yang, S.M. Strittmatter, The reticulons: a family of proteins with diverse functions, Genome Biol. 8 (2007) 234.
[2] T. Oertle, M.E. Schwab, Nogo and its partners, Trends Cell Biol. 13 (4) (2003) 187–194.
[3] S.H. Park, C. Blackstone, Further assembly required: construction and dynamics of the endoplasmic reticulum network, EMBO Rep. 11 (7) (2010) 515–521.
[4] Y. Liu, S. Vidensky, A.M. Ruggiero, S. Maier, H.H. Sitte, J.D. Rothstein, Reticulon RTN2B regulates trafficking and function of neuronal glutamate transporter EAAC1, J. Biol. Chem. 283 (10) (2008) 6561–6571.
[5] P. Steiner, K. Kulangara, J.C.F. Sarria, L. Glauser, R. Regazzi, H. Hirling, Reticulon 1-C/neuroendocrine-specific protein-C interacts with SNARE proteins, J. Neurochem. 89 (3) (2004) 569–580.
[6] G. Montenegro, A.P. Rebelo, J. Connell, R. Allison, C. Babalini, M.D. Aloia, P. Montieri, R. Schüle, H. Ishiura, J. Price, A. Strickland, M.A. Gonzalez, L. Baumbach-Reardon, T. Deconinck, J. Huang, G. Bernardi, J.M. Vance, M.T. Rogers, S. Tsuji, P. De Jonghe, M.A. Pericak-Vance, L. Schöls, A. Orlacchio, E. Reid, S. Züchner, Mutations in the ER-shaping protein reticulon 2 cause the axon-degenerative disorder hereditary spastic paraplegia type 12, J. Clin. Invest. 122 (2012) 538–544.
[7] W. He, Y. Lu, I. Qahwash, X.-Y. Hu, A. Chang, R. Yan, Reticulon family members modulate BACE1 activity and amyloid-beta peptide generation, Nat. Med. 10 (9) (2004) 959–965.
[8] S. Tagami, Y. Eguchi, M. Kinoshita, M. Takeda, Y. Tsujimoto, A novel protein, RTN-XS, interacts with both Bcl-XL and Bcl-2 on endoplasmic reticulum and reduces their anti-apoptotic activity, Oncogene 19 (50) (2000) 5736–5746.
[9] F. Di Sano, B. Fazi, G. Citro, P.E. Lovat, G. Cesareni, M. Piacentini, Glucosylceramide synthase and its functional interaction with RTN-1C regulate chemotherapeutic-induced apoptosis in neuroepithelioma cells, Cancer Res. 63 (14) (2003) 3860–3865.
[10] M.E. Schwab, Functions of Nogo proteins and their receptors in the nervous system, Nat. Rev. Neurosci. 11 (12) (2010) 799–811.
[11] H.J. van de Velde, A.J. Roebroek, F.W. van Leeuwen, W.J. Van de Ven, Molecular analysis of expression in rat brain of NSP-A, a novel neuroendocrine-specific protein of the endoplasmic reticulum, Brain Res. Mol. Brain Res. 23 (1–2) (1994) 81–92.
[12] H.J. van de Velde, A.J. Roebroek, N.H. Senden, F.C. Ramaekers, W.J. Van de Ven, NSP-encoded reticulons, neuroendocrine proteins of a novel gene family associated with membranes of the endoplasmic reticulum, J. Cell Sci. 107 (1994) 2403–2416.
[13] A.U. Mannan, J. Boehm, S.M. Sauter, A. Rauber, P.C. Byrne, J. Neesen, W. Engel, Spastin, the most commonly mutated protein in hereditary spastic paraplegia interacts with Reticulon 1 an endoplasmic reticulum protein, Neurogenetics 7 (2) (2006) 93–103.
[14] X. Zhao, J. Jäntti, Functional characterization of the trans-membrane domain interactions of the Sec61 protein translocation complex beta-subunit, BMC Cell Biol. 10 (2009) 76.
[15] J. Iwahashi, N. Hamada, Human reticulon 1-A and 1-B interact with a medium chain of the AP-2 adaptor complex, Cell. Mol. Biol. 49 (6) (2003) 467–471.
[16] G. Giannini, A. Conti, S. Mammarella, M. Scrobogna, V. Sorrentino, The ryanodine receptor/calcium channel genes are widely and differentially expressed in murine brain and peripheral tissues, J. Cell Biol. 128 (5) (1995) 893–904.
[17] K. Tully, S.N. Treistman, Distinct intracellular calcium profiles following influx through N- *versus* L-type calcium channels: role of Ca^{2+}-induced Ca^{2+} release, J. Neurophysiol. 92 (2004) 135–143.
[18] V. Sorrentino, R. Rizzuto, Molecular genetics of Ca(2+) stores and intracellular Ca(2+) signalling, Trends Pharmacol. Sci. 22 (9) (2001) 459–464.
[19] X. Liu, M.J. Betzenhauser, S. Reiken, A.C. Meli, W. Xie, B.X. Chen, O. Arancio, A.R. Marks, Role of leaky neuronal ryanodine receptors in stress-induced cognitive dysfunction, Cell 150 (5) (2012) 1055–1067.
[20] M. Zhao, P. Li, X. Li, L. Zhang, R.J. Winkfein, S.R. Chen, Molecular identification of the ryanodine receptor pore-forming segment, J. Biol. Chem. 274 (37) (1999) 25971–25974.
[21] J. Nakai, T. Ogura, F. Protasi, C. Franzini-Armstrong, P.D. Allen, K.G. Beam, Functional nonequality of the cardiac and skeletal ryanodine receptors, Proc. Natl. Acad. Sci. U. S. A. 94 (3) (1997) 1019–1022.
[22] T. Oertle, M.E. van der Haar, C.E. Bandtlow, A. Robeva, P. Burfeind, A. Buss, A.B. Huber, M. Simonen, L. Schnell, C. Brösamle, K. Kaupmann, R. Vallon, M.E. Schwab, Nogo-A inhibits neurite outgrowth and cell spreading with three discrete regions, J. Neurosci. 23 (13) (2003) 5393–5406.
[23] H. Blum, H. Beier, H.J. Gross, Improved silver staining of plant proteins, RNA and DNA in polyacrylamide gels, Electrophoresis 8 (2) (1987) 93–99.
[24] A. Shevchenko, M. Wilm, O. Vorm, M. Mann, Mass spectrometric sequencing of proteins silver-stained polyacrylamide gels, Anal. Chem. 68 (5) (1996) 850–858.
[25] R. Arnitz, B. Sarg, H.W. Ott, A. Neher, H. Lindner, M. Nagl, Protein sites of attack of N-chlorotaurine in Escherichia coli, Proteomics 6 (2006) 865–869.
[26] C. Chen, H. Okayama, High-efficiency transformation of mammalian cells by plasmid DNA, Mol. Cell. Biol. 7 (8) (1987) 2745–2752.
[27] R. Schindl, H. Kahr, I. Graz, K. Groschner, C. Romanin, Store depletion-activated CaT1 currents in rat basophilic leukemia mast cells are inhibited by 2-aminoethoxydiphenyl borate. Evidence for a regulatory component that controls activation of both CaT1 and CRAC (Ca(2+) release-activated Ca(2+) channel) channels, J. Biol. Chem. 277 (2002) 26950–26958.
[28] D. Jiang, R. Wang, B. Xiao, H. Kong, D.J. Hunt, P. Choi, L. Zhang, S.R. Chen, Enhanced store overload-induced Ca2+ release and channel sensitivity to luminal Ca2+ activation are common defects of RyR2 mutations linked to ventricular tachycardia and sudden death, Circ. Res. 97 (2005) 1173–1181.
[29] C.A. Sailer, H. Hu, W.A. Kaufmann, M. Trieb, C. Schwarzer, J.F. Storm, H.-G. Knaus, Regional differences in distribution and functional expression of small-conductance Ca^{2+}-activated K^+ channels in rat brain, J. Neurosci. 22 (22) (2002) 9698–9707.
[30] D.J. West, E.C. Smith, A.J. Williams, A novel and rapid approach to isolating functional ryanodine receptors, Biochem. Biophys. Res. Commun. 294 (2) (2002) 402–407.
[31] S. Zissimopoulos, D.J. West, A.J. Williams, F.A. Lai, Ryanodine receptor interaction with the SNARE-associated protein snapin, J. Cell Sci. 119 (2006) 2386–2397.
[32] F.A. Lai, M. Dent, C. Wickenden, L. Xu, G. Kumari, M. Misra, H.B. Lee, M. Sar, G. Meissner, Expression of a cardiac $Ca^{(2+)}$-release channel isoform in mammalian brain, Biochem. J. 288 (1992) 553–564.
[33] Y. Ouyang, T.J. Deerinck, P.D. Walton, J.A. Airey, J.L. Sutko, M.H. Ellisman, Distribution of ryanodine receptors in the chicken central nervous system, Brain Res. 620 (2) (1993) 269–280.
[34] M.A. Dent, G. Raisman, F.A. Lai, Expression of type 1 inositol 1,4,5-trisphosphate receptor during axogenesis and synaptic contact in the central and peripheral nervous system of developing rat, Development 122 (1996) 1029–1039.
[35] T. Nakagawa, H. Okano, T. Furuichi, J. Aruga, K. Mikoshiba, The subtypes of the mouse inositol 1,4,5-trisphosphate receptor are expressed in a tissue-specific and developmentally specific manner, Proc. Natl. Acad. Sci. U. S. A. 88 (1991) 6244–6248.
[36] D.A. Dodd, B. Niederoest, S. Bloechlinger, L. Dupuis, J.P. Loeffler, M.E. Schwab, Nogo-A, -B, and -C are found on the cell surface and interact together in many different cell types, J. Biol. Chem. 280 (13) (2005) 12494–12502.
[37] Y. Shibata, C. Voss, J.M. Rist, J. Hu, T.A. Rapoport, W.A. Prinz, G.K. Voeltz, The reticulon and DP1/Yop1p proteins form immobile oligomers in the tubular endoplasmic reticulum, J. Biol. Chem. 283 (27) (2008) 18892–18904.
[38] N. Zurek, L. Sparks, G. Voeltz, Reticulon short hairpin transmembrane domains are used to shape ER tubules, Traffic 3 (2011) 28–41.
[39] P.S. McPherson, K.P. Campbell, Characterization of the major brain form of the ryanodine receptor/Ca^{2+} release channel, J. Biol. Chem. 268 (26) (1993) 19785–19790.
[40] H. Shimizu, M. Fukaya, M. Yamasaki, M. Watanabe, T. Manabe, H. Kamiya, Use-dependent amplification of presynaptic Ca^{2+} signaling by axonal ryanodine receptors at the hippocampal mossy fiber synapse, Proc. Natl. Acad. Sci. U. S. A. 105 (33) (2008) 11998–12003.
[41] R. Bull, J.P. Finkelstein, J. Gálvez, G. Sánchez, P. Donoso, M.I. Behrens, C. Hidalgo, Ischemia enhances activation by Ca^{2+} and redox modification of ryanodine receptor channels from rat brain cortex, J. Neurosci. 28 (38) (2008) 9463–9472.
[42] F. Lai, M. Misra, L. Xu, A. Smith, G. Meissner, The ryanodine receptor Ca^{2+}-release channel complex of skeletal muscle sarcoplasmic reticulum: evidence for a cooperatively coupled, negatively charged homotetramer, J. Biol. Chem. 264 (28) (1989) 16776–16785.
[43] R.A. Padua, W.H. Wan, J.I. Nagy, J.D. Geiger, [3H]ryanodine binding sites in rat brain demonstrated by membrane binding and autoradiography, Brain Res. 542 (1) (1991) 135–140.
[44] R.A. Padua, J.I. Nagy, J.D. Geiger, Subcellular localization of ryanodine receptors in rat brain, Eur. J. Pharmacol. 298 (2) (1996) 185–189.
[45] I. Zimanyi, I.N. Pessah, Pharmacological characterization of the specific binding of [3H]ryanodine to rat brain microsomal membranes, Brain Res. 561 (2) (1991) 181–191.
[46] T. Murayama, Y. Ogawa, Similar Ca^{2+} dependences of [3H]ryanodine binding to α- and β-ryanodine receptors purified from bullfrog skeletal muscle in an isotonic medium, FEBS Lett. 380 (3) (1996) 267–271.
[47] R. Bull, J.P. Finkelstein, A. Humeres, M.I. Behrens, C. Hidalgo, Effects of ATP, Mg^{2+}, and redox agents on the Ca^{2+} dependence of RyR channels from rat brain cortex, Am. J. Physiol. Cell Physiol. 293 (1) (2007) 162–171.
[48] D.M. Balshaw, N. Yamaguchi, G. Meissner, Modulation of intracellular calcium-release channels by calmodulin, J. Membr. Biol. 185 (1) (2002) 1–8.
[49] G.K. Voeltz, W. Prinz, Y. Shibata, J.M. Rist, T.A. Rapoport, A class of membrane proteins shaping the tubular endoplasmic reticulum, Cell 124 (3) (2006) 573–586.
[50] I. Sparkes, N. Tolley, I. Aller, J. Svozil, A. Osterrieder, S. Botchway, C. Mueller, et al., Five Arabidopsis reticulon isoforms share endoplasmic reticulum location, topology, and membrane-shaping properties, Plant Cell 22 (4) (2010) 1333–1343.
[51] M.G. Chelu, C.I. Danila, C.P. Gilman, S.L. Hamilton, Regulation of ryanodine receptors by FK506 binding proteins, Trends Cardiovasc. Med. 14 (6) (2004) 227–234.
[52] T. Jayaraman, A.M. Brillantes, A.P. Timerman, S. Fleischer, H. Erdjument-Bromage, P. Tempst, A.R. Marks, FK506 binding protein associated with the calcium release channel (ryanodine receptor), J. Biol. Chem. 267 (14) (1992) 9474–9477.

[53] A.P. Timerman, H. Onoue, H.B. Xin, S. Barg, J. Copello, G. Wiederrecht, S. Fleischer, Selective binding of FKBP12.6 by the cardiac ryanodine receptor, J. Biol. Chem. 271 (34) (1996) 20385–20391.
[54] X.H.T. Wehrens, S.E. Lehnart, S.R. Reiken, S.-X. Deng, J.A. Vest, D. Cervantes, J. Coromilas, D.W. Landry, A.R. Marks, Protection from cardiac arrhythmia through ryanodine receptor-stabilizing protein calstabin 2, Science 304 (2004) 292–296.
[55] T. GrandPré, F. Nakamura, T. Vartanian, S.M. Strittmatter, Identification of the Nogo inhibitor of axon regeneration as a Reticulon protein, Nature 403 (2000) 439–444.
[56] X. Wang, S.J. Chun, H. Treloar, T. Vartanian, C.A. Greer, S.M. Strittmatter, Localization of Nogo-A and Nogo-66 receptor proteins at sites of axon-myelin and synaptic contact, J. Neurosci. 22 (13) (2002) 5505–5515.
[57] J. Laurén, F. Hu, J. Chin, J. Liao, M.S. Airaksinen, S.M. Strittmatter, Characterization of myelin ligand complexes with neuronal Nogo-66 receptor family members, J. Biol. Chem. 282 (8) (2007) 5715–5725.
[58] T. Furuichi, D. Furutama, Y. Hakamata, J. Nakai, H. Takeshima, K. Mikoshiba, Multiple types of ryanodine receptor/Ca2+ release channels are differentially expressed in rabbit brain, J. Neurosci. 14 (8) (1994) 4794–4805.
[59] Y.M. Usachev, S.A. Thayer, All-or-none Ca2+ release from intracellular stores triggered by Ca2+ influx through voltage-gated Ca2+ channels in rat sensory neurons, J. Neurosci. 17 (19) (1997) 7404–7414.
[60] D.L. Gruol, J.G. Netzeband, K.L. Parsons, Ca2+ signaling pathways linked to glutamate receptor activation in the somatic and dendritic regions of cultured cerebellar purkinje neurons, J. Neurophysiol. 76 (5) (1996) 3325–3340.
[61] E.D. Martín, W. Buño, Caffeine-mediated presynaptic long-term potentiation in hippocampal CA1 pyramidal neurons, J. Neurophysiol. 89 (6) (2003) 3029–3038.
[62] S. Sajikumar, Q. Li, W.C. Abraham, Z.C. Xiao, Priming of short-term potentiation and synaptic tagging/capture mechanisms by ryanodine receptor activation in rat hippocampal CA1, Learn. Mem. 16 (3) (2009) 178–186.
[63] W. Zhao, N. Meiri, H. Xu, S. Cavallaro, A. Quattrone, L. Zhang, D.L. Alkon, Spatial learning induced changes in expression of the ryanodine type II receptor in the rat hippocampus, FASEB J. 14 (2) (2000) 290–300.
[64] K. Kobayashi, T. Manabe, T. Takahashi, Calcium-dependent mechanisms involved in presynaptic long-term depression at the hippocampal mossy fibre-CA3 synapse, Eur. J. Neurosci. 11 (1999) 1633–1638.
[65] Y. Wang, M.J. Rowan, R. Anwyl, Ryanodine produces a low frequency stimulation-induced NMDA receptor-independent long-term potentiation in the rat dentate gyrus *in vitro*, J. Physiol. 495 (1996) 755–767.
[66] M. Reyes, P.K. Stanton, Induction of hippocampal long-term depression requires release of Ca2+ from separate presynaptic and postsynaptic intracellular stores, J. Neurosci. 16 (19) (1996) 5951–5960.
[67] T. Adasme, P. Haeger, A.C. Paula-Lima, I. Espinoza, M.M. Casas-Alarcón, M.A. Carrasco, C. Hidalgo, Involvement of ryanodine receptors in neurotrophin-induced hippocampal synaptic plasticity and spatial memory formation, Proc. Natl. Acad. Sci. U. S. A. 108 (7) (2011) 3029–3034.
[68] J.C. Gant, K.C. Chen, C.M. Norris, I. Kadish, O. Thibault, E.M. Blalock, N.M. Porter, P.W. Landfield, Disrupting function of FK506-binding protein 1b/12.6 induces the Ca^{2+}-dysregulation aging phenotype in hippocampal neurons, J. Neurosci. 31 (5) (2011) 1693–1703.